 SDHM, vol.6, no.3, pp.213-238, 2010

Crack Growth Modeling for Mixed-mode Problems

A.P.Cisilino[1] and M.H. Aliabadi[2]

Abstract: This paper presents a review of the dual boundary element method for modeling crack growth in two-dimensional and three-dimensional mixed mode problems. The modeling strategy for crack coalescence using the DBEM is presented and comparisons are made with alternative solutions where available. Also presented are three-dimensional multiple crack growth and microcrack growth problems.

Keywords: Dual Boundary Element Method, Fatigue Crack growth

1 Introduction

Crack growth processes in the context of linear elastic fracture mechanics are normally modeled with an incremental crack-extension analysis. For each increment of crack-extension stress intensity factors are evaluated as the key fracture parameter. The direction of the crack growth, and in the case of fatigue, the amount of crack extension per load cycle, are directly linked to the value of the stress intensity factors. For general mixed-mode conditions, numerical methods must be used for the evaluation of the stress intensity factors as well as modeling the often complex continuously changing geometry due to the extension of the crack.

Early attempts to model crack growth using the Finite Element Method (FEM) can be traced back to works of Shephard et al (1985), Valliappan and Marti (1985), Swenson and Ingraffea (1988), Remiz and Blackburn (1990) and O'Donoghue et al (1995). More recent advances in the finite element method can be found in the work of Theilig et al (1997,1999) for two-dimensional mixed-mode crack problems, and, Schoellman et al (2002), Buchholz and Richard (2004a, 200b), Cittarella and Buchholz (2007) and Li et al (2010) for three–dimensional mixed-mode problems. Another recent successful application of the FEM to mixed-model crack growth modeling is due to the development of eXtended Finite Element Method

[1] INTEMA, Faculty of Engineering, Universidad Nacional de Mar del Plata – CONICET, Av. Juan B. Justo 4302, Mar del Plata, Argentina.
[2] Department of Aeronautics, Imperial College London, South Kensington, London, SW7 2BZ, UK.

(XFEM). The XFEM as developed by Black and Belytscho (1999) and Rethore et al (2005) is inspired by the enriched finite elements originally proposed by Benzely (1974) and Foschi and Barrett(1976) (see Aliabadi and Rooke (1991) for an overview of enriched FEM).

A robust method for modeling crack growth in general mixed-mode problems was developed by Portela, et al (1993). The method was an extension of the Dual Boundary Element Method earlier proposed by Portela, Aliabadi and Rooke (1992) as an effective way of modeling crack problems using the boundary integral equation. The DBEM for the first time allowed modeling mixed-mode crack problems without a need for continuous remeshing and user interferences. The crack extension was modeled with new boundary elements without having to remesh the previous crack geometry. The extension of the DBEM to different linear, transient and nonlinear problems can be found in Letião, et al (1995), Aliabadi and Sollero (1998), Saleh and Aliabadi (1995), Prasad et al (1996), Dell Erba and Aliabadi (2000) and Wen et al (2004).

Another interesting development in 3D crack growth modeling is the coupled symmetric Galerkin boundary element method formulation with FEM alternating method as presented by Nishikov et al (2001), Han and Atluri (2002) and Atluri (2005).

In this paper the DBEM method is reviewed for two and three dimensional mixed mode crack problems. Next, the extension of the method to modeling crack coalescence is presented. The application of the DBEM to microcrack modeling and mixed modeling are also presented and comparisons are made with alternative solutions where possible.

2 The Dual Boundary Element Method

The Dual Boundary Element Method (DBEM) overcomes the mathematical degeneration of the classical BEM formulation when applied to crack problems where the two crack surfaces are coplanar. The DBEM uses two independent boundary integral equations, with the displacement equation applied for collocation on one of the crack surfaces and the traction equation on the other. Upon the model discretization and the application of the boundary conditions, the traction and displacement boundary integral equations are used to set up a system of equations to solve the boundary unknowns (Portela et al, 1992 and Mi and Aliabadi, 1992)).

The application of the classical DBEM formulation as introduced by Portela et al (1992) and Mi and Aliabadi (1992) required discretization of both crack surfaces. The continuity requirements for the displacement and traction fields makes necessary to use the so-called "discontinuous elements" on the crack surfaces. Discontinuous elements use two set of nodes: the geometric nodes which define which define

the geometry of the model, and the collocation nodes which are used to interpolate the field variables (displacement and tractions). For problems requiring large number of elements on the crack surfaces or involving many cracks the above approach can lead to more degrees of freedom than absolutely necessary. An alternative approach to mitigate this problem is to formulate the displacement and the traction boundary integral equations in terms of the relative displacements between the crack surfaces. In this way, the number of nodes associated to the crack discretization is halved, since only one of the cracks surfaces is discretized (see for instance Cisilino and Aliabadi, 2004). The crack surface displacements are obtained after the problem solution by postprocessing the boundary data. Figure 1 illustrates the details of the crack discretization strategy for two and three-dimensional problems. The change required to the classical DBEM formulation (and the corresponding software) to include the crack displacement discontinuity instead of crack surface displacements is trivial. Recently, Benedetti et al (2008) have made significant speed up of the solution process for the DBEM by implementing a fast solver.

For the details of the mathematical formulation of the DBEM and its implementation for two and three-dimensional problems the reader is referred to the works by Portela et al (1993) and Mi and Aliabadi (1995), respectively.

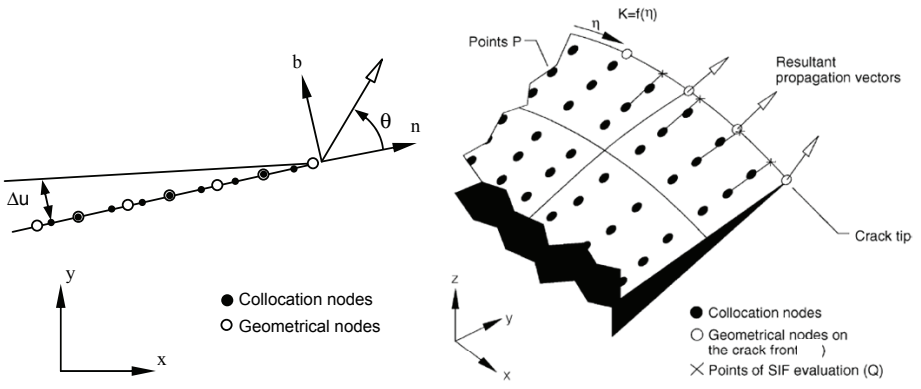

(*a*) (*b*)

Figure 1: Crack discretization for the DBEM for (a) two dimensional and (b) three-dimensional problems.

3 Fatigue crack propagation analysis

3.1 Stress Intensity Factor computation

Accurate evaluation of crack tip stress intensity factors, K, is of most importance for the effective analysis of crack propagation problems. Stress intensity factors are computed in this work by using the so-called one-point displacement formula, in which the relative displacements of the crack surfaces, Δu, calculated from the DBEM model are used in the near-crack-tip stress field equations to obtain the local mixed-mode K values (see Aliabadi and Rooke, 1991). This technique was preferred to path and domain integral methodologies, which although very accurate and efficient (see Portela et al, 1992 and Cisilino et al, 1998) cannot be easily adapted to solve close interacting cracks due to the difficulties to define the integration paths or domains.

The expressions for the computation of stress intensity factors using a one-point formula for the case of a general three-dimensional mixed-mode problem are

$$\begin{aligned} K_I &= \frac{E}{4(1-\nu^2)}\sqrt{\frac{\pi}{2r}}\Delta u_b \\ K_{II} &= \frac{E}{4(1-\nu^2)}\sqrt{\frac{\pi}{2r}}\Delta u_n \\ K_{III} &= \frac{E}{4(1-\nu^2)}\sqrt{\frac{\pi}{2r}}\Delta u_t \end{aligned} \tag{1}$$

where E is the Young's modulus, ν the Poisson's ratio and r is the distance from the crack front to the collocation node, P, where the relative displacements between the crack surfaces are computed. The terms Δu_n, Δu_b, Δu_t and are the projections of the relative displacements on the local coordinate directions (i.e. normal, binormal and tangential) at the crack front (see Figure 1).

The efficiency of the one-point displacement formula strongly depends on the accuracy of the displacements calculated on the crack surface. This is ensured in this work by using special crack-tip elements that exhibit the correct $\sqrt{r}$ variation for the displacement field. Details of its implementation and performance can be found in Aliabadi and Rooke (1991) and Ortiz et al (2001b).

The application of the one-point formula is straight forward for two-dimensional problems (note that only K_I and K_{II} are computed). In this case the relative displacements Δu_n and Δu_b in Eq. (1) are those of the collocation nodes closer to the crack tip. On the other hand, a more elaborated procedure is necessary for the three dimensional problems: the relative displacements of the second-closer line of collocation nodes to the crack front are used for the evaluation of Eq. (1); and

the distances r from the collocation points to the crack front are measured in directions perpendicular to the crack front (see Figure 1*b*). The resulting stress intensity factors are assigned to the points Q, which are located at the intersections of the distance vectors r with the crack front. Finally, the K-results at the geometrical nodes are calculated by extrapolating the K-values assigned to the Q points.

4 Crack extension

The crack extension is modeled incrementally, assuming a piece-wise linear discretization of the unknown crack path. The magnitude and direction of crack increments are computed from the K results.

Figure 2 depicts the typical fatigue crack growth behavior in metals (Sih, 1991). The schematic log-log plot presents the rate of crack growth per load cycle, *da/dN*, as a function of the applied stress intensity factor range, $\Delta K = K_{max} - K_{min}$. The sigmoidal curve contains three distinct regions. In Region I, crack growth goes asymptotically to zero as ΔK approaches a threshold value, ΔK_{th}. This means that for stress intensity factors below ΔK_{th} there is no crack growth, i.e. there is a fatigue limit. The threshold effect is believed to be caused by a number of different processes, which lead to crack blocking. In Region II, the log *da/dN* tends to vary linearly with respect to the log of ΔK, what results in a stable crack growth. Finally, the crack propagation rate accelerates dramatically in Region III as ΔK approaches the material fracture toughness K_c.

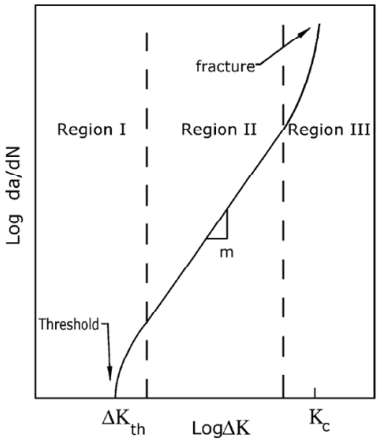

Figure 2: Typical fatigue crack growth behavior in metals fatigue crack growth behaviour in metals.

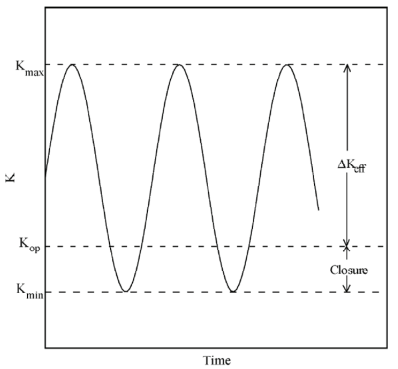

Figure 3: Definition of the stress intensity factor range.

The study cases presented in this work are devoted to model crack growth in the near-threshold (Region I) and stable crack (Region II) regimes. Crack growth is Region II can be predicted using the well-known formula developed by Paris et al (1961)

$$\frac{da}{dN} = C\Delta K^n, \tag{2}$$

where C and n are empirical material constants which may also depend on load frequency, environment and the mean load $R = K_{min}/K_{max}$ (see Figure 3). The R is considered via the closure effect (Elber, 1970). Crack closure decreases the fatigue crack growth rate by reducing the effective stress intensity range. Due to a number of causes, like plasticity, crack roughness or material transformations (see Figure 4) the crack faces are in contact bellow K_{op} (see Figure 3) and the crack does not propagate. Following Elber (1970) an effective stress intensity factor range is defined:

$$\Delta K_{eff} = K_{max} - K_{op} \tag{3}$$

together with an effective stress intensity ratio:

$$U = \frac{\Delta K_{\text{eff}}}{\Delta K} = \frac{K_{max} - K_{op}}{K_{max} - K_{min}}. \tag{4}$$

Crack growth is Region I is modeled using the formula by Klesnil and Lucas (1972), which is a variation of the Paris' law introduced in Eq. (2) which accounts for the near-threshold regime:

$$\frac{da}{dN} = C\left(\Delta K^m - \Delta K_{\text{th}}^{\text{m}}\right), \tag{5}$$

where C and m are material constants. The effect of closure can be introduced in Eq. (5) by replacing the term ΔK^m by ΔK_{eff}^m. For multiple crack fatigue crack growth problems Salgado and Aliabadi (1998) presented a formula where the relative magnitude of the stress intensity factors at different crack tips in linked to the amount of crack extension.

The length of the crack extension is computed using Eq. (2) or (5) incrementally, this is by approximating $da/dN \approx \Delta a/\Delta N$. In this way, the crack extension ΔK is calculated for each propagation step after setting a number of load cycles ΔN. It is worth noting that in order to use Eq. (2) or (5) it is necessary to compute an equivalent stress intensity factor range which combines the effects of the three crack-modes into a single ΔK value. This is done using the formula proposed by Gerstle (1986):

$$\Delta K = \left(\Delta K_{\text{I}} + \text{B}\left|\Delta K_{\text{III}}\right|\right)^2 + 2\Delta K_{\text{II}}^2. \tag{6}$$

The constant B takes values between zero and unity. Dirgantara and Aliabadi (2000) proposed linking the constant B to a formula which included relative values of the stress intensity factors for bending and membrane for thin wall structures.

Among the several available criteria for computing the local direction of crack growth, the minimum strain energy criterion due to Sih (1991) is used in this work. This criterion states that the direction of crack growth at any point along the crack front is towards the region with the minimum value of the strain density factor S. The strain density factor S can be written in terms of the stress intensity factors as follows:

$$S = a_{11}K_I^2 + 2a_{12}K_IK_{II} + a_{22}K_{II}^2 + a_{33}K_{III}^2 \tag{7}$$

where a_{11}, a_{12}, a_{22} and a_{33} are trigonometric polynomials of $sin(\theta)$ and $cos(\theta)$ being θ the direction of the crack extension in the local coordinate system (see Figure 1). The propagation angle θ is obtained by replacing the computed mixed-mode K values in Eq. (7) and comparing the values of $S(\theta)$ at stationary points $d^2S(\theta)/d^2\theta > 0$. This is done numerically by using the bisection method.

The results for the propagation length and direction are used to compute the propagation vectors along the crack front (or at the crack tip for the two-dimensional case). The crack surface is extended by adding new elements along the crack front. The dimensions and spatial orientation of these new elements are those given by the propagation vectors. It is worth to note that this procedure does not need of the model remeshing when dealing with two-dimensional problems or three-dimensional embedded cracks. Some local remeshing is needed only when dealing with surface cracks in three-dimensional analyses or with crack coalescence problems. The full details about the model update procedure including the strategy for reassembling of the BEM system of equations for the new geometry can be found in the works by Portela et al (1993) and Cisilino and Aliabadi (2004) for the two- and three-dimensional cases respectively.

5 Crack coalescence

In order to complete an assessment of crack propagation, it is necessary to define a criterion for the coalescence of fatigue cracks from adjacent damage sites. The simplest possible coalescence criterion would be to assume that ligament failure occurs only when the physical crack tips meet. This condition does not take into account the plasticity developing between the crack tips. Collins and Cartwright (1996) showed that a prediction based on the elastic criterion is in reasonable agreement with the experimental evidence for the early stages of crack growth only. The predictions become increasingly inaccurate in the later stages where plastic flow at the crack tips would be more prevalent.

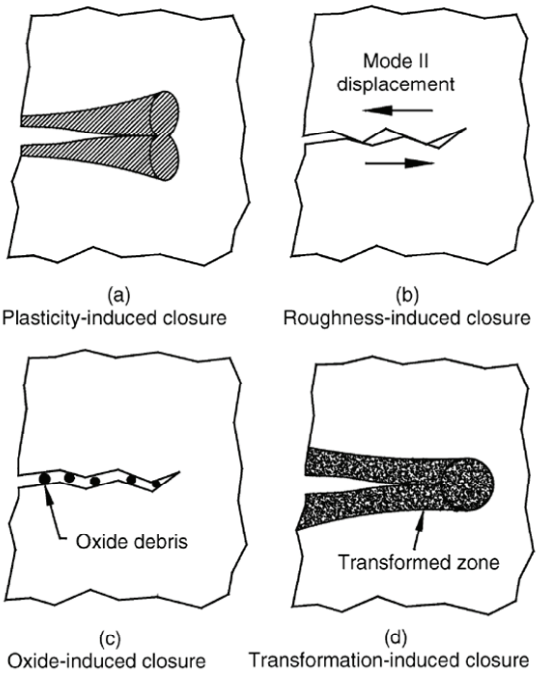

Figure 4: Fatigue crack closure mechanisms.

Among the models reported in the literature that due to Swift (1992) is used in this work to account for the effect of plasticity. (a comprehensive review and discussion of those models can be found in Caballero Pinto, 2006). Swift's criterion states that a ligament between two adjacent cracks will fail if the sum of the radius of crack-tip plastic zones equals the ligament size. This is:

$$r_p(a) + r_p(b) = L \tag{8}$$

where $r_p(a)$ and $r_p(b)$ are the radius of the plastic zones in front of each crack-tip and L is the ligament size (see Figure 5).

Various models and formulas have been used to estimate the plastic zone radius. Following Swift (1992) the Irwin's formula is used in this work:

$$r_p = \frac{1}{2\pi}\left(\frac{K}{\sigma_Y}\right)^2 \tag{9}$$

where σ_Y is the material yield stress. In Equation (10) sometimes a local link-up stress defined as $\sigma_0 = (\sigma_{UT} + \sigma_y)/2$ is used in place of σ_Y.

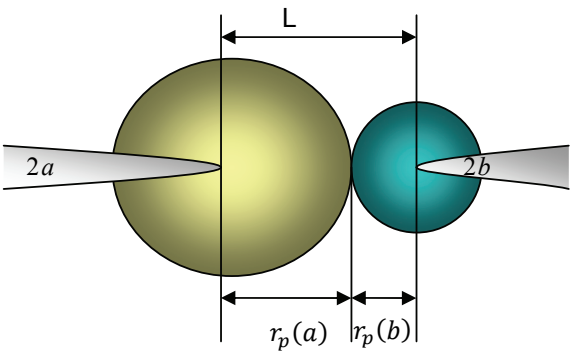

Figure 5: Touching plastic zones as a criterion for ligament failure.

A similar criterion can be used to detect a crack touching a free boundary. In this sense, Silva et al (2000) considered that a link-up between the crack and the free surface takes place when the distance between the crack tip and the free boundary is equal to the crack plastic zone radius.

In the present implementation the distances from each crack tip to the free boundaries, crack paths and other crack tips are checked in every crack extension increment. These distances are compared to the radius of the crack-tip plastic zone computed using Equation (10). In the case that the plastic zones touch each other or a free boundary, a model remeshing is performed in order to update the problem geometry. For the details of the remeshing procedure see Caballero Pinto (2006).

6 Study cases

6.1 Micromechanics of fatigue crack growth in austempered ductile iron

The ADI (Austempered Ductile Iron) belongs to the family of spheroidal graphite cast irons. ADI combines good elongation and toughness with high tensile strength; combination that increases the resistance to wear and fatigue when compared to other ductile irons. The material has a wide range of industrial applications, as is the case of chain wheels, lines of cement mills, railroad wheels, gears and automotive crankshafts. The prominent properties of ADI are consequence of its matrix microstructure, obtained by a thermal treatment called austempering. ADI microconstituents are reacted austenite (enriched in carbon), retained austenite (unreacted) and acicular ferrite. Minor amounts of martensite and carbides may also be present. The quantity and size of graphite nodules, matrix phases formed dur-

ing thermal treatment, and alloy content influence this microstructure, denominated ausferrite (Gundlach and Janowak, 1991).

The relationship between fatigue crack growth and matrix microstructure is the focus of previous work by Greno et al (1999). A quantitative study of the morphology of fatigue crack growth proved that the crack path preferentially intersects graphite nodules, and that a microcracking process takes place in the region of high stress concentration around the tip of the main crack. Graphite-matrix interfaces are extremely irregular, with sharp corners that in some cases constitute imminent microcracks that emanate from the nodules. Ultimately, the main crack advances by interaction and coalescence of the microcracks, as shown in Figure 6. It is proposed that as microcracks simultaneously propagate besides the main crack, the available elastic energy for the propagation of the main crack is lowered mainly because of the creation of a larger crack surface. This reduces the general rate of advance and in some cases causes the premature arrest of crack growth. The above-mentioned mechanism provides evidence to explain the relatively low propagation rates and high effective propagation threshold values for this material.

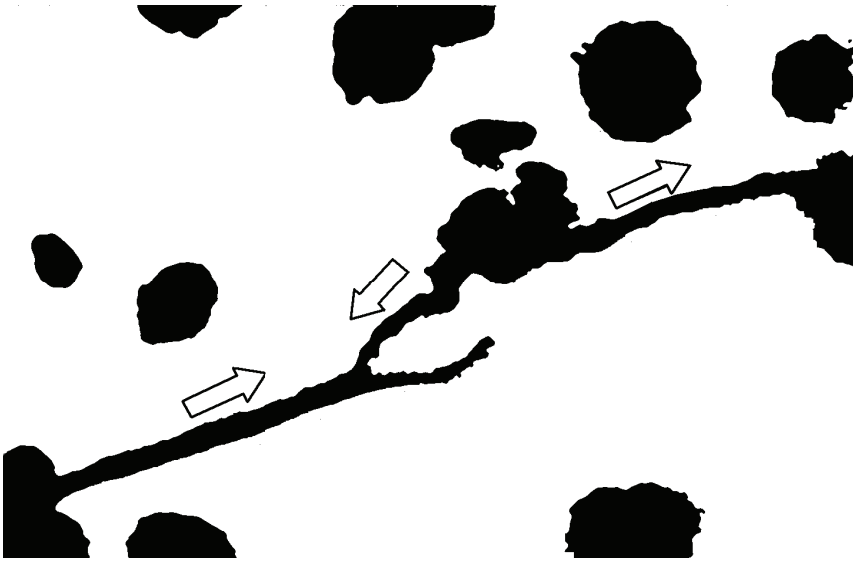

Figure 6: Enlarged 500 micrograph showing the fatigue crack propagation mechanism in ADI (from Greno et al, 1999).

In what follows two-dimensional DBEM modeling is used to assess the micromechanics of fatigue crack growth in ADI in order to study the crack-microcrack interaction mechanism.

Crack closure is a relevant factor when assessing the mechanism of fatigue crack propagation in ADI as it behaves differently for macrocracks and microcracks. In this sense it is worth to note that while closure levels can be significant for macrocracks, microcracks could be almost closure free (Leis et al, 1986).

A simple model consisting in a large main crack and a microcracked nodule is considered first. The model geometry and discretization are shown in Figure 7 together with the resulting propagation paths for three closure levels. The length of the main crack was initially set to be forty times that of the microcracks. Microcracks were placed to coincide with the 'equator' of the nodule, where the maximum principal stresses develop. As for all models presented in this work, graphite nodules were assimilated to circular voids. This assumption implies to consider a material with 100% nodularity, and to neglect the mechanical response of graphite when compared with that of the metal matrix. The metal matrix is assumed to be isotropic and linear elastic. The propagation law due to Klesnil and Lucas (1972) (see, Eq. (5)) for the near threshold regime was used. Material constants were taken from Greno et al (1999) and they were C=4.43.10^{-10}, m=2.85 and ΔK_{th}=5 MPa$\sqrt{\text{m}}$. Closure levels were selected as U=1 (no closure), U=0.6 and U=0, the last one corresponding to a limiting case for which the main crack did not propagate. Loading configuration was remote tension, with a load level set in such a way that initial ΔK values for the microcracks were close to the propagation threshold ΔK_{th}.

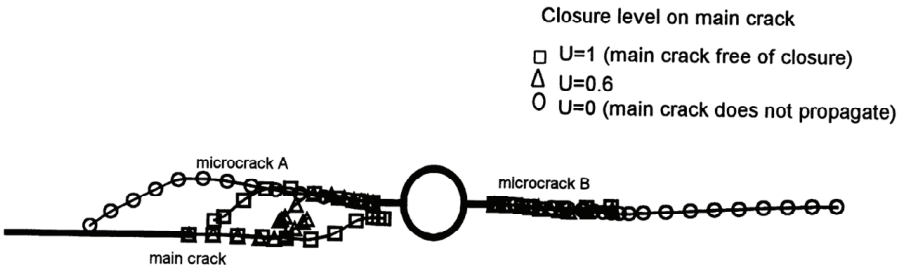

Figure 7: Effect of the closure level on the crack-microcrack interaction mechanism.

Figure 8 illustrates the evolution of ΔK with load cycles N for the results in Figure 7. Stress intensity factor ranges ΔK are normalized with respect to ΔK_{th}, in such a way that values greater than one represent propagating cracks, and values below one stand for non-propagating cracks. Note that as the main crack approaches the microcrack emanating from the nodule, interaction effects cause a substantial increment in ΔK at crack tip A, which propagates in opposite direction to the main crack

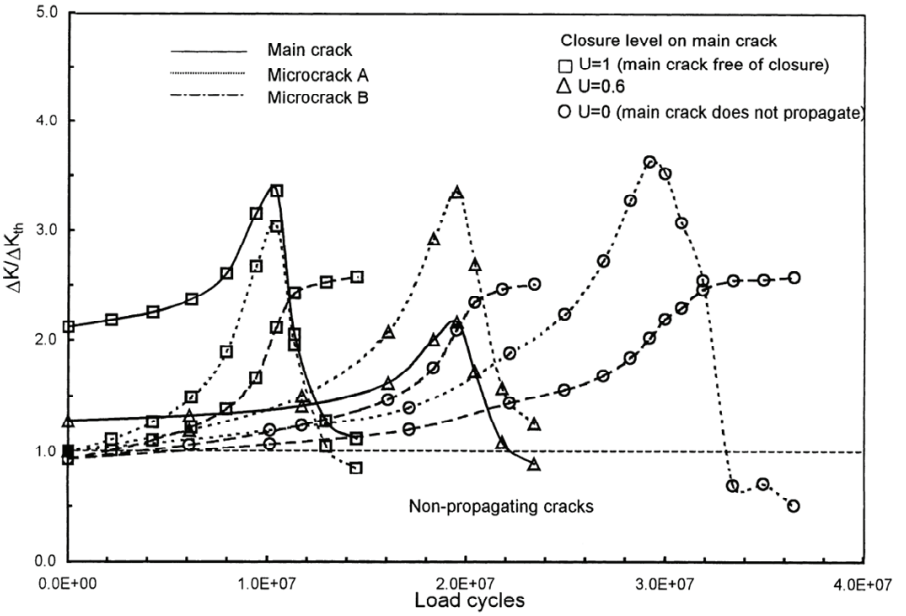

Figure 8: Evolution of ΔK with the number of load cycles.

growth until joining it. As soon as the main crack and the first microcrack coalesce, microcrack B on the opposite side of the nodule becomes dominant, taking the role of the main crack. The above mechanism validates the theoretical model proposed by Greno et al (1999). The effect of closure is of delaying the process, since as the main crack propagation rate slows down, the coalescence with the microcrack takes longer.

A more general situation is illustrated in Figure 9, where a main crack propagates into an array of randomly distributed nodules with equatorial microcracks, labelled from A to H. Obtained results allow to extend the propagation mechanism of the previous example, as the tips B, D, F and H successively take the role of main crack tip. At the same time, microcracks A, C, E and G propagate towards the main crack tip, to finally become dormant due to load shielding effects. Microcracks I, J, K and L do not take part in the main propagation path, however they present the same general behaviour as the other microcracks. In this case more than one microcrack propagate simultaneously towards the tip of the dominant crack, justifying the presence of the 'bifurcations' observed by Greno et al (1999).

A complete analysis of the micromechanics of crack propagation in ADI can be found in the paper by Ortiz et al (2001a) where the DBEM results presented here

were complemented with a statistical analysis in order to estimate their deviation bounds. Besides, the shielding effect of microcracking on the main crack was studied using a continuum mechanics approach. The effects of the microstructure topology on the fracture toughness of dual-phase ADI were studied by Basso et al (2010) by means of finite element modeling and experimental testing.

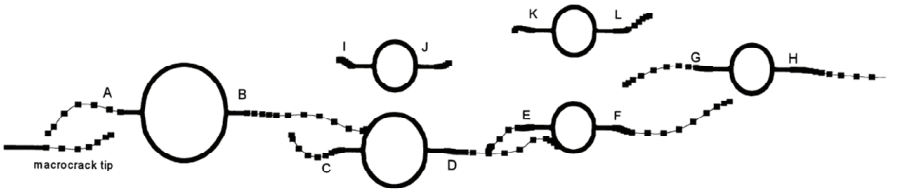

Figure 9: Propagation paths for general a general nodule array.

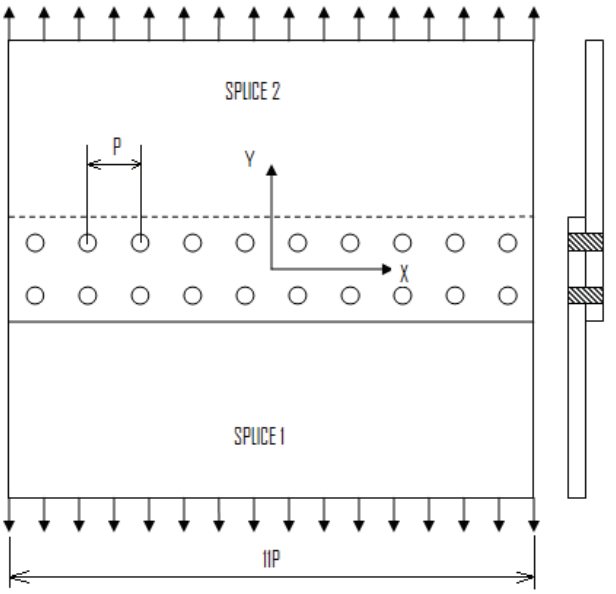

Figure 10: Schematic of lap joint configuration.

Recently Sfantos and Aliabadi (2007) have presented a mutliscale boundary element methodology for modeling crack growth. The method takes into account two different scales of micro and macro and links the process through average volume theory.

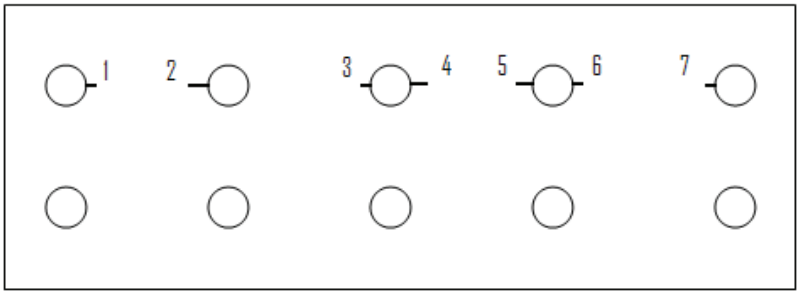

Figure 11: Lap joint splice with seven small cracks emanating from fastener holes.

6.2 Bonded, riveted lap-joint in a fuselage

The phenomenon of multiple cracks of arbitrary lengths emanating from a row of fastener holes in a bonded, riveted lap joint in a pressurized fuselage of a class of airplanes has been the object of a number of studies in assessing the structural integrity of aging airplanes.

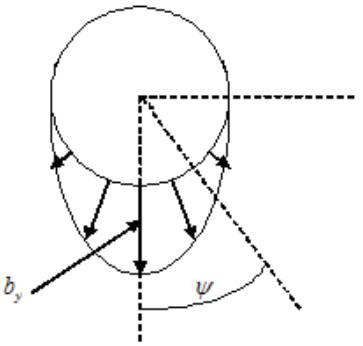

Figure 12: A fastener hole with bearing stress distributed along the lower portion of the boundary.

The problem studied in this example contains two lines of fasteners of radius r=2 mm and pitch p=25.4 mm (see Figure 10). The distance from the fasteners to the edges of the splices is equal to $p/2$. Each splice is 1.6 mm thick and is made of aluminum 2024-T3 with elastic modulus E=73000 MPa, Poison's ratio ν=0.33 and yield strength σ_Y=320 MN/m^2. The splice 1 contains seven small cracks emanating from the fastener holes in the upper line as illustrated in Figure 11. Cracks 1, 3, 6

and 7 have initial sizes $r/4$ and cracks 2, 4 and 5 have initial sizes $r/2$.

The joint is loaded in the y-direction with σ=69 MPa. For the local analysis, only one sheet (splice 1) is modelled. Following Park and Atluri (1993) the forces at the fastener holes are distributed according to the formula (see Figure 12):

$$b_r = \frac{3b_y}{4rh} cos^2, \tag{10}$$

where b_y= 1400 N is the load carried by each fastener, h is the splice thickness and ψ is the angle indicating the position along the hole boundary.

Displacement boundary conditions u_y=0 are applied at the top of the splice, while the condition u_x=0 is specified along the right and the left edges in order to simulate a much longer joint. Crack propagation analysis is performed assuming cyclic loading of constant amplitude with R=0. Paris' constants are C=0.183$\times 10^{-11}$ and n=3.284.

Figure 13 shows the evolution of the crack paths together with the σ_{yy} stress contours. Results are shown for the initial geometry and after 21 and 22 crack extension increments. After the 22^{th} extension increment the plastic radius of crack tips 4 and 5 touched, so they merged in a single crack.

Mode I stress intensity factors, normalized with respect to $K_0 = \sigma\sqrt{\pi r}$ are presented in Figure 14 as a function of the number of loading cycles. Due to the nature of the applied load (almost perpendicular to the crack directions) the Mode II stress intensity factor are very low.

6.3 Propagation of three-dimensional multiple surface cracks

Generally speaking, fatigue cracks will almost always be initiated at the surface, from regions of high-stress concentration due to changes in geometry or geometric discontinuities created during fabrication. This is for instance the typical situation of a welded structure, where the small weld defects enhance crack growth even from the first few stress cycles. It is presented in this section the modeling of the interaction and propagation of two identical semicircular surface cracks located on parallel planes. Propagation is modeled in the stable regime (Region II in Figure 2) using the Paris' Law in Eq. (2). Material constants are set C=3.10$\times 10^{-10}$ and n=2.92.

Figure 15 illustrates the model geometry and load configuration for the parallel cracks. The model dimensions are scaled to the crack radius a. Figure 16 is a rear view of the specimen where some of the boundary elements on its lateral face have been removed to show the cracks more clearly. Crack geometries correspond to those resulting after five propagation increments with N=500 cycles. Also shown

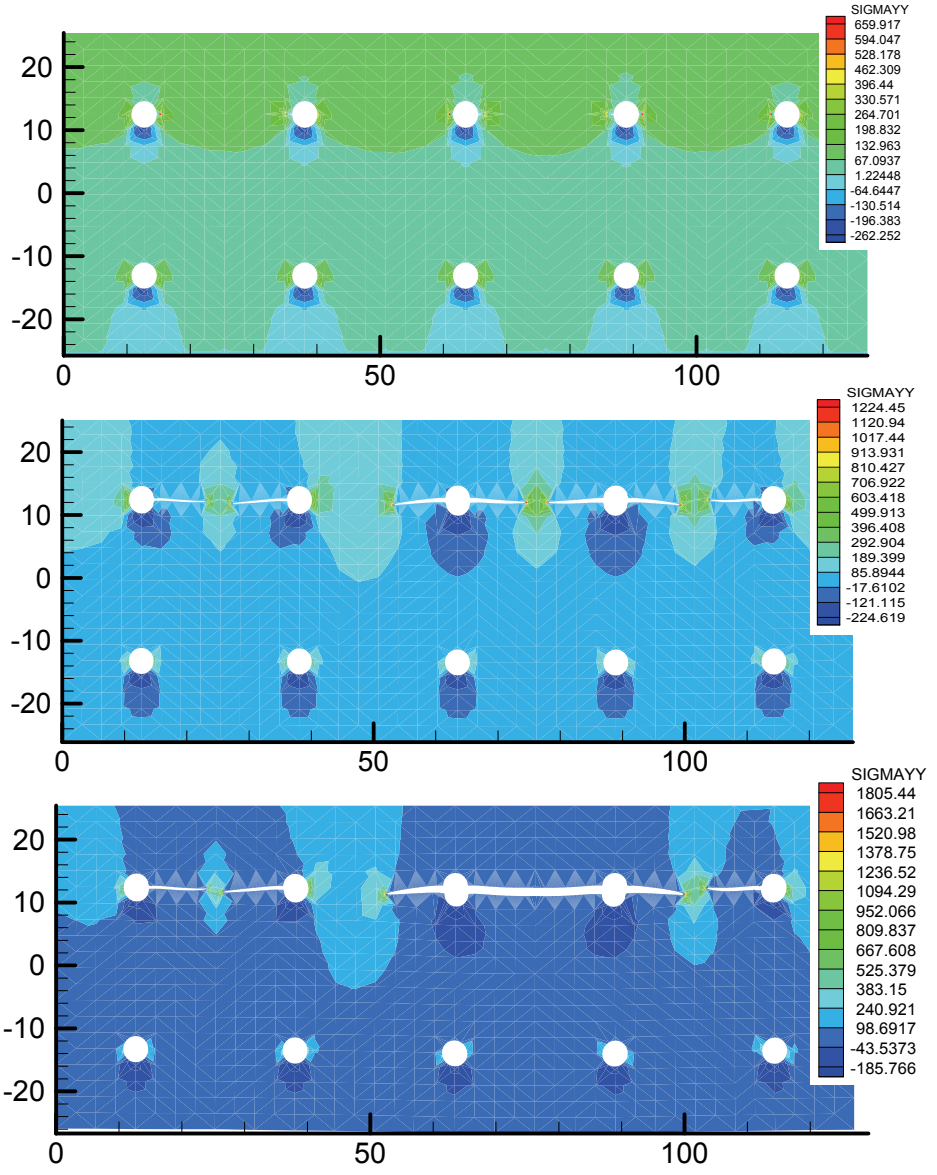

Figure 13: Evolution of the crack path and the b_y stress with crack propagation: (a) initial geometry, (b) 21th increment, and (c) 22th increment.

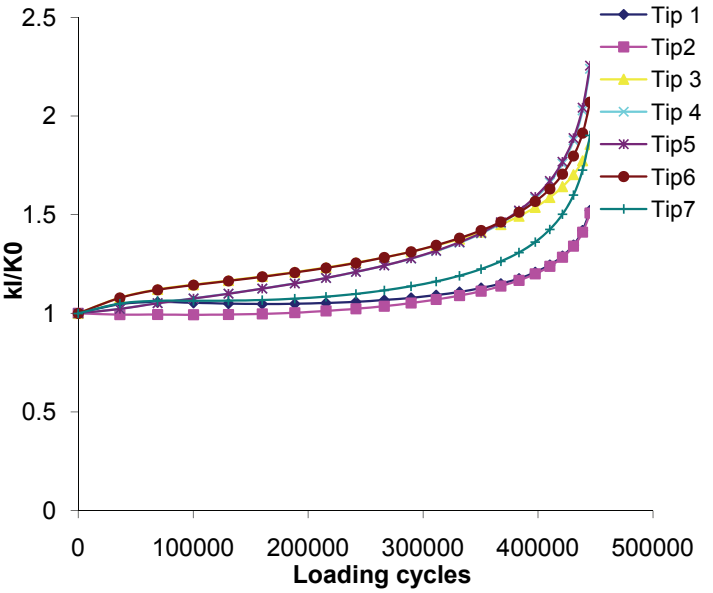

Figure 14: Normalizes Mode-I stress intensity factors as a function of the loading cycles.

in Figure 16 are the discontinuous triangular elements introduced to the model during the automatic remeshing procedure. The sub-figure in the top right-hand corner shows the crack propagation path on the free surface.

The results obtained are in good agreement with the crack path behaviour observed in experiments. Soboyejo et al (1990) and the authors also noted a deviation of the adjacent cracks tips as they approached each other, see Figure 17.

The evolution of the stress intensity factor components ΔK_I, ΔK_{II} and ΔK_{III} along the crack fronts are plotted for both cracks in Figures 18, 19 and 20. The normalized position on the crack front is given by the ratio between the distance η, measured from the crack tips labeled A in Figure 15, and the total crack front length ℓ. The results in the figures show that the behaviour of ΔK_I was almost unaffected by the presence of the second crack for the first two propagation increments. , However, after the third increment, when the adjacent tips passed each other, a shielding effect took place and ΔK_I values dramatically decreased. In contrast to ΔK_I; ΔK_{II} values were early influenced by the presence of the second crack. Their absolute values started at a maximum and they decreased after the second crack extension. Note that the asymmetric evolution in the values of ΔK_{II} made the cracks grow towards each other. On the other hand, the absolute value of ΔK_{III} monotonously

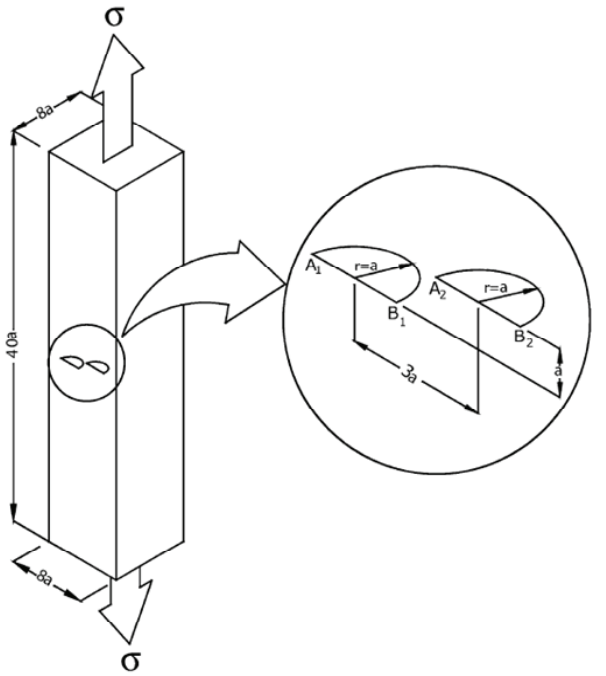

Figure 15: A prismatic bar with two semicircular offset parallel cracks under remote tension.

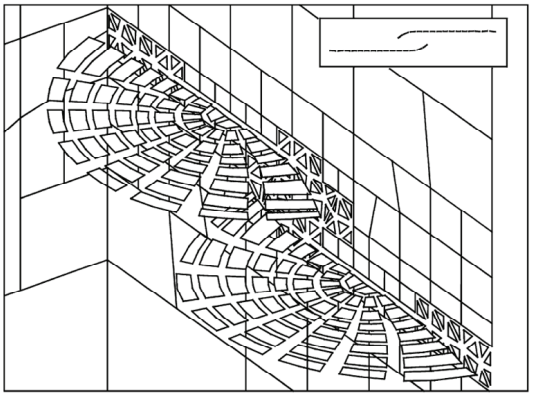

Figure 16: Evolution of the crack geometry during propagation (The triangular elements on the model surface were introduced by the automatic remeshing algorithm).

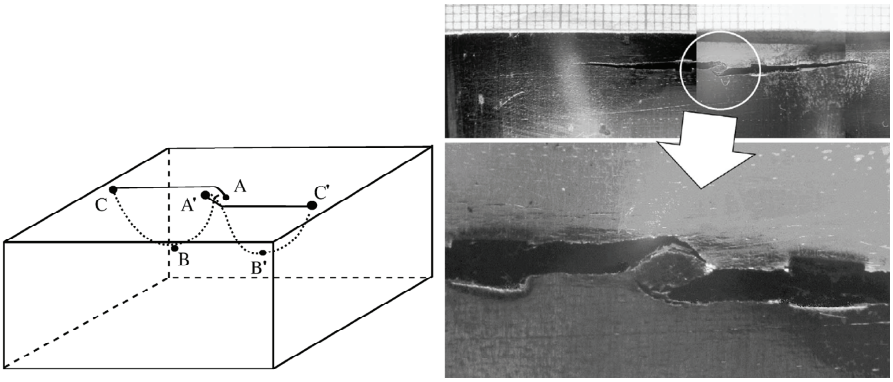

(*a*) (*b*)

Figure 17: Experimental evidence about the deviation of the adjacent crack tips during crack propagation: (a) schematic due to Soboyejo et al (1990) and (b) experiments by the authors.

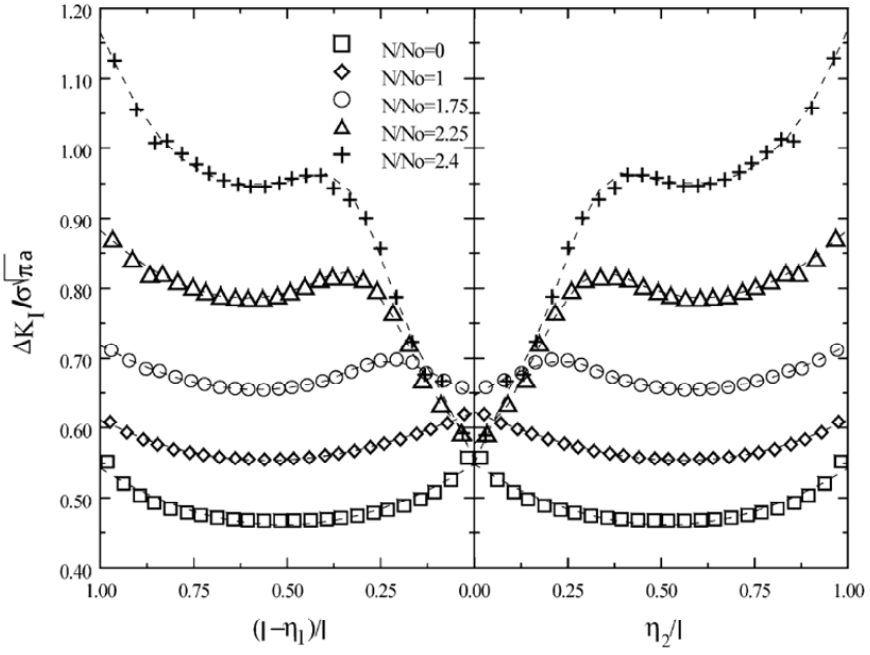

Figure 18: Evolution of ΔK_I along the crack front with the extension increments.

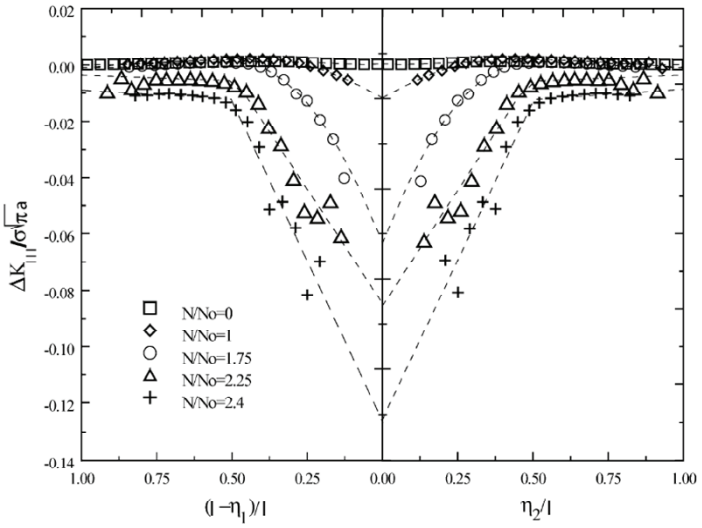

Figure 19: Evolution of ΔK_{II} along the crack front with the extension increments.

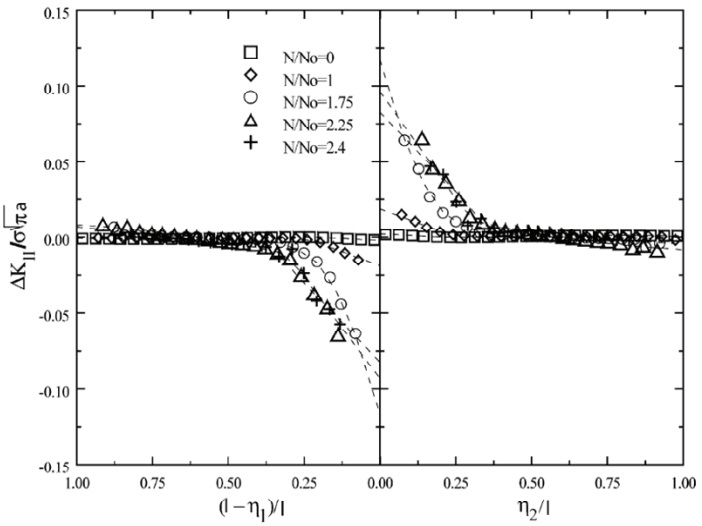

Figure 20: Evolution of ΔK_{III} along the crack front with the extension increments.

increased throughout the propagation analysis. However, these values were small when compared to ΔK_I and ΔK_{II}.

Further examples on the modeling of three dimensional cracks with the DBEM can be found in the works by Cisilino and Aliabadi (1997, 1999, 2004) and Wessel et al (2001). These papers include comparisons with numerical experiments and also results for elastoplastic DBEM crack propagation analysis.

7 Conclusions

In this paper the application of the dual boundary element method to crack growth and coalescence was presented. It was shown that the method can be effectively used to model multiple site damage for two-dimensional and three-dimensional problems.

Acknowledgement: We would like to acknowledge the contribution of Mr J Pinto Caballero in running some of the 2D simulations. The first author thanks the financial support by the Agencia de Promoción Científica y Tecnológica de la República Argentina and the Universidad Nacional de Mar del Plata via the research grant PICT N' 1154.

References

Aliabadi, M.H. and Rooke, D.P. (1991): Numerical Fracture Mechanics, WIT Press, Southampton, UK.

Aliabadi, M.H. And Sollero, P. (1998) Crack growth analysis in homogeneous orthotropic laminates *Composites Science and Technology*, vol. 58, no. 10, pp. 1697-703.

Atluri, S.N. (2005): Application of DATLE: Damage tolerance analysis and life enhancement [3D non-plannar fatigue crack growth], SID, *Structural Integrity and Durability*, vol. 1, no. 1., pp. 1-20.

Benedetti, I., Aliabadi, M.H. and Davi, G. (2008): A fast 3D dual boundary element method based on hierarchical matrices. *International Journal of Solids and Structures*, vol. 45, no. 7-8, pp. 2355-76.

Black, T. and Belytscchko, T. (1999) Elastic crack growth in finite elements with minimal remeshing, *International Journal for Numerical Methods in Engineering*, vol. 45, pp. 601-620

Basso, A., Martinez, R., Cisilino, A.P. and Sikora, J. (2010): Experimental and numerical assessment of fracture toughness of dual-phase austempered ductile iron, *Fatigue & Fracture of Engineering Materials & Structures*, vol. 33, pp. 1–11.

Benzley, S.E. (1974): Representation of singularities with isoparametric finite elements, *International Journal for Numerical Methods in Engineering*, vol. 8, pp. 1333-1336.

Buchholz, F.G., Richard, H.A. (2004): From Compact Tension Shear (CTS) to All Fracture modes (AFM) Specimen and Loading Devices, *Proc. of the Int. Conf. on Advances in Structural Integrity* (ICASI2004), Bangalore, India.

Buchholz, F.G., Chergui, A. and Richard, H.A. (2004): Fracture analyses and experimental results of crack growth under general mixed mode loading conditions. *Engineering Fracture Mechanics*, vol. 71, pp. 455-468.

Cisilino, A.P. and Aliabadi, M.H. (1997): Three-dimensional BEM analysis for fatigue crack growth in welded components. *International Journal of Pressure Vessels and Piping*, vol. 70, no. 2, pp. 135-144.

Cisilino, A.P., Aliabadi, M.H. and Otegui, J.L. (1998): Energy domain integral applied to solve centre and double-edge crack problems in three dimensions, *Theoretical and Applied Fracture Mechanics*, vol. 29, pp. 181-194.

Cisilino, A.P. and Aliabadi, M.H. (1999): Three-dimensional boundary element analysis of fatigue crack growth in linear and non-linear fracture mechanics, *Engineering Fracture Mechanics*, vol. 63, pp. 713-733.

Cisilino, A.P. and Aliabadi, M.H. (2004): Dual boundary element assessment of three-dimensional fatigue crack growth. *Engineering Analysis with Boundary Elements*, vol. 28, no. 9, pp. 1157-1173.

Cittarella, R. and Buchholz F.G. (2007): Comparison of DBEM and FEM crack path predictions with experimental findings for a SEN-specimen under anti-plane shear loading, *Key Engineering Materials*, vols. 348-349, pp. 129-132.

Collins R.A. and Cartwrigth D.J. (1996): On the development of the strip yield model for the assessment of multiple site damage. *Theoretical and Applied Fracture Mechanics*, vol. no. 25, pp. 167-178.

Dell'Erba, D.N. and Aliabadi M.H. (2000): Three-dimensional thermo-mechanical fatigue crack growth using BEM *International Journal of Fatigue*, vol. 22, no. 4, pp. 261-273.

Dirgantara, T. and Aliabadi, M.H. (2000): Crack growth analysis of plates loaded by bending and tension using dual boundary element method *International Journal of Fracture*, vol. 105, no. 1, pp. 27-47.

Dhondt, G. (1998): Cutting of 3-D finite element mesh for automatic mode I crack propagation calculation. *Int. J. Num. Meth. Engng*. 42, 749-772.

Elber, W. (1970): Fatigue crack closure under cyclic tension, *Engineering Fracture Mechanics*, vol. 29, pp. 37–45.

Fedelinski, P., Aliabadi, M.H. and Rooke, D.P. (1997): The time-domain DBEM for rapidly growing cracks *International Journal for Numerical Methods in Engineering*, vol. 40, no. 9, pp. 1555-1572

Foschi, R.O. and Barrett,J.D. (1976): Stress intensity factors in anisotropic plates using singular elements, International Journal for Numerical Methods in Engineering, vol. 10, pp. 1281-1287.

Fulland, M., Sander, M., Kullmer, G. and Richard, H. A. (2008): Analysis of fatigue crack propagation in the frame of a hydraulic pressure. *Engineering Fracture Mechanics*, vol. **75**, pp. 892-900.

Gerstle, W.H. (1986): *Finite and Boundary Element Modeling of Crack Propagation in Two- and Three-Dimensions Using Interactive Computer Graphics*, PhD Thesis, Cornell University, Ithaca, USA.

Greno G.L., Otegui J.L. and Boeri R.E., (1999): Mechanisms of fatigue crack growth in Austempered Ductile Iron, *International Journal of Fracture*, vol. 21, pp. 35-43.

Gundlach, R.B. and Janowak J.F. (1991): A review of austempered ductile iron metallurgy, *Proceedings of the American Foundrymen's Society*, World Conference on Austempered Ductile Iron, pp.1-10.

Han, Z.D. and Atluri, S.N. (2002): SGBEM (for cracked local domain)-FEM (for uncracked global structure) alternating method for analyzing 3D surface cracks and their fatigue-growth, *Computer Modeling in Engineering and Sciences,* vol. 3, no. 6, pp. 699-716.

Klesnil, M. and Lukas, P. (1972): Influence of strength and stress history on growth and stabilisation of fatigue cracks, *Engineering Fracture Mechanics*, vol. 4, pp. 77-92.

Leis, B.N., Hoper, A.T. and Ahmad, J. (1986): Critical review of the fatigue growth of short cracks, *Engineering Fracture Mechanics*, vol. 23, no. 25, pp. 883-898.

Leitao, V.M.A., Aliabadi, M.H. and Rooke, D.P. (1995): Elastoplastic simulation of fatigue crack growth dual boundary element formulation *International Journal of Fatigue*, vol. 17, no. 5, pp. 353-363.

Li Qing-Fen, Zhu Li, Buchholz F-G and Yan Sheng-Yuan (2010): Computational analysis of the AFM specimen on mixed-mode II and III fracture. *Key Engineering Materials*, vols. 452-453, pp. 173-176.

Mi, Y. and Aliabadi, M.H. (1992): Dual boundary element method for three-dimensional fracture mechanics analysis. Engineering Analysis with Boundary Elements, vol. 10, no. 2, pp. 161-171.

Mi, Y and Aliabadi, M.H. (1995): An automatic procedure for mixed-mode crack growth analysis, *Communications in Numerical Methods in Engineering*, vol. 11, no. 2, pp. 167-77

Nikshikov, G.P., Parks, J.H and Atluri, S.N. (2001): SGBEM-FEM alternating method for analyzing 3D non-planar cracks and their growth in structural components. *Computer Modeling in Engineering & Sciences,* vol. 2, no. 3, pp. 401-22.

O'Donoghue, P.E., Atluri, S.N. and Pipkins, D.S. (1995): Computational strategies for fatigue crack growth in three dimensions with application to aircraft components. *Engineering Fracture Mechanics*, vol. 52, no.1, pp. 51-64.

Ortiz, J., Cisilino, A.P. and Otegui, J.L. (2001a): Effect of microcracking on the micromechanics of fatigue crack growth in austempered ductile iron, *Fatigue and Fracture of Engineering Materials and Structures*, vol. 24, no. 9, pp. 591-605.

Ortiz, J., Cisilino, A.P. and Otegui J.L. (2001b): Boundary element analysis of fatigue crack propagation micromechanisms in ductile iron, *Engineering Analysis with Boundary Elements*, vol. 25, pp. 467-473.

Paris, P.C., Gomez M.P. and Anderson, W.P. (1961): A rational analytic theory of fatigue. *The Trend in Engineering*, vol. 13, pp. 9–14.

Park, J.H., Atluri, S.N. (1993): Fatigue growth of multiple-cracks near a row of fastener-holes in a fuselage lap-joint. *Computational Mechanics*, vol. 13, pp. 189-203.

Portela, A., Aliabadi M.H., Rooke D.P. (1993): The dual boundary element method: effective implementation for crack problems. *International Journal for Numerical Methods in Engineering*, vol. 33, no. 6, pp. 1269-87.

Portela, A., Aliabadi, M.H., Rooke, D.P. (1993): Dual boundary element incremental analysis of crack propagation. Computers and Structures, vol. 46, no. 2, pp. 237-247.

Prasad, N.N.V., Aliabadi, M.H. and Rooke, D.P. (1996): Thermomechanical fatigue crack growth. *International Journal of Fatigue*, vol. 18, no. 6, pp. 349-361.

Remzi,E.M. and Blackburn,W.S (1990): Automatic crack propagation studies in T-junction and cross bars. *Engineering Computations,* vol. 7, pp. 116-124.

Rethore, J., Gravouil, A. and Combescure (2005): An energy-conserving scheme for dynamic crack growth using the eXtended finite element method. *International Journal for Numerical Methods in Engineering*, vol. 63, pp. 631-659.

Richard, H.A., Linning, W. and Henn, K. (1991): Fatigue crack propagation under combined loading. *Forensic Engineering*, vol. 3, no. 2/3, pp. 99-109.

Saleh, A.L. and Aliabadi, M.H.(1995): Crack growth analysis in concrete using boundary element method. *Engineering Fracture Mechanics*, vol. 51, no. 4, pp.

533-545.

Salgado, N.K. and Aliabadi, M.H. (1998): Boundary element analysis of fatigue crack propagation in stiffened panels. *Journal of Aircraft*, vol. 35, no. 1, pp. 122-130.

Sfantos, G.K. and Aliabadi, M.H. (2007): Multi-scale boundary element modelling of material degradation and fracture. *Computer Methods in Applied Mechanics and Engineering*, vol. 196, no. 7, pp. 1310-1329.

Shepard, M.S., Yehia, N.A.B, Burd, G.S. and Weidner, T.J. (1985): Automatic crack propagation tracking. *Computers and Structures*, vol. 20, pp. 211-223.

Sih, G.C. (1991): Mechanics of Fracture Initiation and Propagation, Kluwer Academic Publishers.

Silva, L.F.M., Go'alves, J.P.M., Oliveira, F.M.F. and de Castr,o P.M.S.T. (2000): Multiple-site damage in riveted lap-joints: experimental simulation and finite element prediction. *International Journal of Fatigue*, vol. 22, pp. 319-338.

Soboyejo, W.O., Knott, J.F., Walsh, M.J. and Cropper, K.R. (1990): Fatigue crack propagation of coplanar semi-elliptical cracks in pure bending, *Engineering Fracture Mechanics*, vol. 37, no. 2, pp. 323–40.

Swenson, D.V. and Ingraffea, A.R. (1988): Modeling mixed mode dynamic crack propagation using finite elements theory and applications. *Computational Mechanics*, vol 3, pp. 381-397.

Swift, T. (1992): Damage Tolerance Capability, in Specialists Conference on Fatigue of Aircraft Materials, Delft University of Technology.

Theilig, H., Doering, R. and Buchholz, F.G. (1997): Higher order fatigue crack path simulation by the MVCCI-method. In B.L. Karihaloo et al (eds), *Advances in Fracture Research*, Pergamon Press, Amsterdam, vol. 4, pp. 2235-2242.

Theilig, H. and Buchholz, F.G. (1999): Crack path prediction by MVCCI-method and experimental verification for specimens under proportional bending and shear loading. In C. Garcia Garino et al (eds), *Mecanica Computacional,* Asociaci'n Argentina de Mec'nica Computcional, Santa Fe, Argentina

Valliappan, S. and Murti,V. (1985): Automatic remeshing technique in quasi-static and dynamic crack propagation. *Proceddings of the NUMETA, 85 Conference.*, pp 107-116.

Wen, P.H., Aliabadi, M.H. and Young, A. (2004): Crack growth analysis for multi-layered airframe structures by boundary element method. *Engineering Fracture Mechanics*, vol. 71, no. 4-6, pp. 619-631.

Wessel, C., Cisilino, A.P., Santi, O., Otegui, J.L., and Chapetti, M. (2001): Numerical and experimental determination of three-dimensional multiple Crack

growth in fatigue, *Theoretical and Applied Fracture Mechanics*, vol. 35, no. 1, pp. 47-58.